Nanoscale

RSCPublishing

PAPER

Selective removal of metallic single-walled carbon nanotubes in full length by organic film-assisted electrical breakdown

Cite this: DOI: 10.1039/x0xx00000x

Keigo Otsuka, Taiki Inoue, Shohei Chiashi* and Shigeo Maruyama*

Received 00th January 2012,
Accepted 00th January 2012

DOI: 10.1039/x0xx00000x

www.rsc.org/nanoscale

An organic film-assisted electrical breakdown technique is proposed to selectively remove metallic (m-) single-walled carbon nanotubes (SWNTs) in full length toward creation of pure semiconducting SWNT arrays which are available for the large-scale fabrication of field effect transistors (FETs). The electrical breakdown of horizontally-aligned SWNT arrays embedded in organic films resulted in a maximum removal length of 16.4 μm. The removal of SWNTs was confirmed using scanning electron microscopy and Raman mapping measurements. The on/off ratios of FETs were improved up to ca. 10,000, similar to that achieved for in-air breakdown. The experimental results indicate that both exothermic oxidation and heat accumulation of the organic films induce the long-length removal of m-SWNTs.

1 Introduction

High-density arrays of semiconducting (s-) single-walled carbon nanotubes (SWNTs) have potential for use in the channels of field-effect transistors (FETs) toward the realization of high-performance logic circuits.[1,2] Although further increase in the SWNT density is required, the horizontal growth of SWNTs with a high degree of alignment has been realized on crystal substrates.[3-6] However, the as-grown SWNT array is a mixture of s- and metallic (m-) SWNTs, which is a major obstacle for FET fabrication using SWNTs, where pure s-SWNT arrays are required. Despite intensive effort, the selective growth of s-SWNTs on substrates[7-10] has not yet attained the required purity (m-SWNTs < 0.0001%[11]). Post-growth separation by wet chemical methods[12-14] has provided ca. 99% purity of s-SWNT and dense, aligned arrays can be assembled after the separation.[14-16] However, fabrication of high on/off ratio devices with sub-micrometer channel length requires the higher purity, and the degree of alignment is needed to be improved. Post-growth removal of m-SWNTs from substrates[2,17-21] has also been studied extensively. Electrical breakdown[2,17] is one of the methods by which m-SWNTs are selectively cut with Joule heating, while the s-SWNTs are preserved through control of the gate voltage. Although electrical breakdown easily yields high on/off ratios for SWNT-FETs by exploiting the difference in the electric transport properties of m- and s-SWNTs, it has a large drawback in scalability. Basically individual FETs must be treated separately because only the hottest short parts (ca. 100 nm) of m-SWNTs are removed by oxidation, while most parts of the m-SWNTs remain after the process, as shown schematically in Figs. 1(a) and 1(b). If the full-length of m-SWNTs that bridge two electrodes could be completely removed, then this provides us an alternative way for fabricating large numbers of FETs without one-by-one treatments. Firstly, temporal electrodes with large widths and a large distance are fabricated on a SWNT arrays only for a m-SWNT removing step, followed by performing a selective removal technique. After that, the remaining pure s-SWNT arrays between the temporal electrodes would be available for further fabrication of a large number of FETs by simply placing electrodes and etching unwanted parts of s-SWNTs. The thermocapillary-induced full length removal technique[21] recently proposed by Jin *et al*. is quite promising, even though the lateral spatial resolution is intrinsically limited by the capillary length scale.

In this work, an organic film-assisted electrical breakdown method was developed to create pure s-SWNT arrays which can be used for a number of FET channels. Electrical breakdown was performed on SWNT arrays covered in organic films to accomplish the full-length removal of m-SWNTs (up to 16.4 μm). This method yielded a high on/off ratio (ca. 10,000) of an FET, which indicates high removal selectivity between s- and m-SWNTs, and also showed fine spatial resolution (ca. 55 nm) in the same way as in-air breakdown.

2 Experimental section

Aligned arrays of SWNTs were grown by the alcohol catalytic chemical vapor deposition method[21] on r-cut crystal quartz substrates.[23,24] The SWNTs were then transferred onto highly p-doped Si substrates with 100-nm-thick SiO_2 layer.[25] Source and drain electrodes were photolithographically defined to conduct currents through SWNTs using sputtering of 5 nm Ti and 50 nm Pd layers, which resulted in back-gated FET structures. FETs with channel widths of 20 μm and various channel lengths (2 to 30 μm) were fabricated. Only FETs with relatively low on/off ratios (less than 10) were used, which contained at least one m-SWNT bridging the source/drain electrodes.

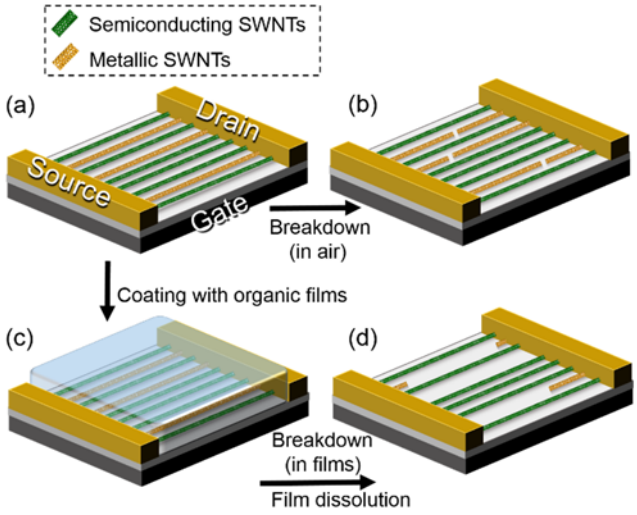

Fig. 1. Schematic illustrations of (a,b) electrical breakdown in air and (a,c,d) electrical breakdown in organic films, respectively. Electrical breakdown in air on (a) an SWNT array with mixtures of s- and m-SWNTs results in (b) partial cutting of the m-SWNTs. In contrast, (c) electrical breakdown in organic films results in the (d) removal of m-SWNTs with longer length. The remaining s-SWNT arrays between the temporal electrodes can be used for further fabrication of a large number of FETs.

Schematic illustrations of organic film-assisted electrical breakdown are shown in Figs. 1(a), 1(c), and 1(d). For organic film-assisted electrical breakdown, SWNT arrays were coated with ca. 50-nm-thick organic films using thermal evaporation or spin-coating [Fig. 1(c)]. Two types of organic material were utilized; α,α,α'-tris(4-hydroxyphenyl)-1-ethyl-4-isopropylbenzene (TCI), hereafter referred to as molecular glass, and the poly(methyl methacrylate) (PMMA; Sigma-Aldrich, MW = ~996,000). The molecular glass is a small-molecule organic material that forms an amorphous thin film. The molecular glass was originally employed to reproduce the thermocapillary-induced process proposed by Jin *et al.*[21] Through such experiments, a simpler technique with fine resolution was achieved using the organic films to enhance SWNT oxidation. In a typical experiment, the drain voltage (V_D) was gradually increased from 0 V at a rate of ca. 0.67 V/min until the drain current (I_D) became sufficiently small, while a positive gate voltage (V_G = +10 V) was applied. This led to selective Joule heating in the m-SWNTs, which resulted in the breakdown of m-SWNTs. Finally, the organic films were removed by immersion of the substrates in acetone to leave pure s-SWNT arrays [Fig. 1(d)].

Electrical breakdown and the transfer characteristics measurement of the FETs were performed under ambient conditions using a semiconductor parameter analyzer (Agilent 4156C). The SWNTs were characterized using scanning electron microscopy (SEM; Hitachi S-4800), atomic force microscopy (AFM; SII SPI3800N), and Raman mapping measurement (Renishaw inVia Raman microscope).

3 Result and discussion

Figures 2(a) and 2(b) show SEM images of a part of an SWNT array before and after electrical breakdown in a molecular glass film, respectively. Figure 2(c) shows the drain current transition during the breakdown process. Partial current drops correspond to the breakdown of SWNTs, and the number of drops is almost the same as the number of broken SWNTs observed with SEM. Among 29 SWNTs connected to both electrodes, 12 SWNTs were fully or partially removed, and this ratio (ca. 41 %) is similar to the typical ratio of m-SWNTs in as-grown SWNTs (ca. 33 %). The transfer characteristics of the FET before and after the breakdown process [Fig. 2(d)] show an increase in the on/off ratio from ca. 2 to 10,000 and a decrease in the on-current by around 90%, which indicates selective removal of the m-SWNTs was achieved. Although the removal lengths ranged from 1.4 to 16.4 μm, the entire length of the SWNT indicated by the red arrow in Figs. 2(a) and 2(b) was removed. The removal length is over 100 times larger than that observed for conventional in-air breakdown (ca. 100 nm).

Breakdown was performed on an SWNT array with close-lying SWNTs [Fig. 2(e)] to estimate the spatial resolution of

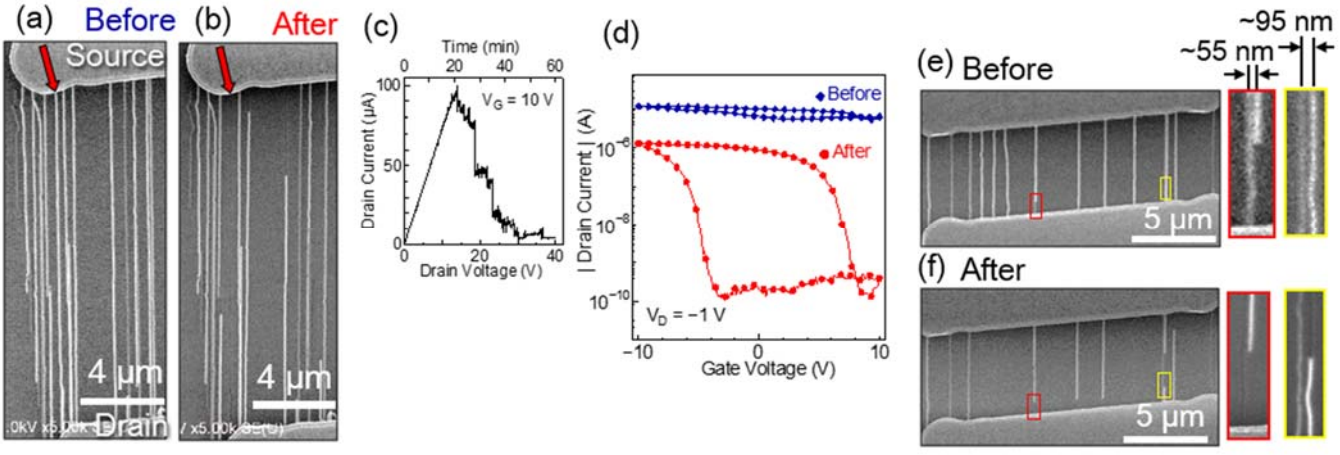

Fig. 2. SEM images of an SWNT array (a) before and (b) after breakdown in molecular glass films. Red arrows indicate an m-SWNT that was removed over its full-length. (c) Drain current transition during the process, where the drain current dropped in accordance with the breakdown of SWNTs. (d) Transfer characteristics of the FET shown in (a,b), which indicate the selective breakdown of m-SWNTs. (e,f) SEM images of an SWNT array that contains closely-placed SWNTs. Close-up images of the outlined regions are inset in (e,f). In those cases, the breakdown of m-SWNTs did not affect adjacent SWNTs.

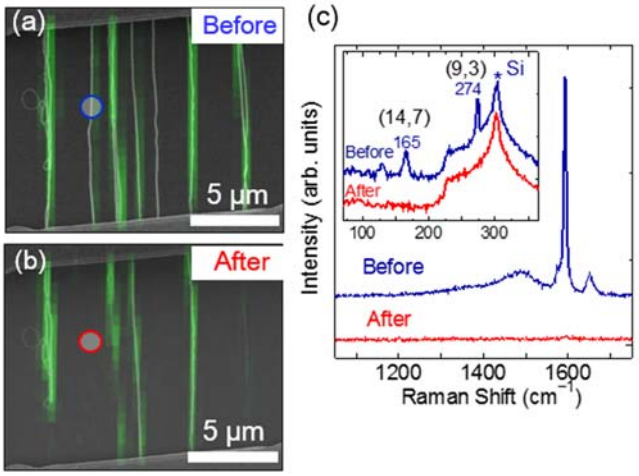

Fig. 3. Superimposed Raman mapping and SEM images of SWNTs (a) before and (b) after the breakdown in a molecular glass film, respectively. Raman mapping images with an excitation wavelength of 532 nm show the integrated intensity of the G-band peaks ranging from 1500 to 1650 cm^{-1}. (c) Raman spectra obtained from identical spots indicated in the SEM images. Inset: RBM spectrum of the SWNTs, which indicates the presence of a bundle of (9,3) and (14,7) SWNTs.

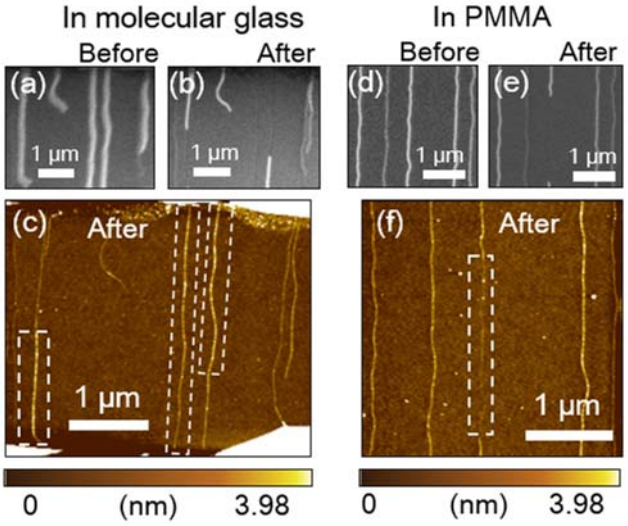

Fig. 4. SEM images of an SWNT array (a) before and (b) after breakdown in a molecular glass film and dissolution of the film, and (c) a corresponding AFM image after these processes. (d-f) Equivalent images for breakdown in a PMMA film. White dashed boxes in the AFM images indicate the removed parts.

organic film-assisted breakdown. The SWNT array shown in Fig. 2(f) was obtained; in the regions outlined by red and yellow lines, the distances between the removed m-SWNTs and the neighboring SWNTs were ca. 55 and 95 nm, respectively. The breakdown of m-SWNTs did not affect the neighboring SWNTs, which suggests that the spatial resolution of the breakdown is better than ca. 55 nm in the case of well-aligned SWNTs. Therefore, this method is potentially applicable to SWNT arrays with densities greater than ca. 18 SWNTs/μm. Considering the thermocapillary-induced purification method yielded the minimum spacing of ca. 250 nm between two parallel and independent trenches[21] and hence can be applied to SWNT arrays with densities up to ca. 8 SWNTs/μm, organic film-assisted electrical breakdown method can be more suitable for the fabrication of FETs with high current driving capability and small gate width.

Raman mapping measurements were performed to confirm the removal of SWNTs, using an excitation laser wavelength of 532 nm. Figures 3(a) and 3(b) show superimposed SEM and G-band mapping images of SWNTs before and after breakdown in a molecular glass film. White lines in the images represent SWNTs observed by SEM and green lines represent the areas from which G-band peaks were obtained. Figure 3(c) shows the G-band and radial breathing mode (RBM) Raman spectra measured at the circled spots indicated in Figs. 3(a) and 3(b). The RBM peaks at 274 and 165 cm^{-1} were assigned as (9,3) chirality (metallic) and (14,7) chirality (semiconducting) under the excitation energy of 2.33 eV (532 nm),[26] respectively. The Raman peaks obtained from the m-SWNT disappeared after breakdown. In this case, the s-SWNT was also removed unintentionally, because it happened to lie very close to the m-SWNT. The disappearance of the white lines from the SEM image and the green lines from the Raman mapping image are clearly consistent, which confirmed the long-length removal of the SWNTs. The Raman observations exclude the possibility of remaining SWNTs which are invisible with SEM due to residual organic materials surrounding the SWNTs or isolation from electron sources (metal electrodes).[27]

Here, we discuss the mechanism of organic film-assisted electrical breakdown, which enables much longer SWNT length removal than that in air. Figures 4(a-c) show SEM images of SWNT arrays before and after electrical breakdown in a molecular glass film and dissolution of the film with acetone, and an AFM image of the arrays after these processes. Figures 4(d-f) show corresponding SEM and AFM images for electrical breakdown in a PMMA film, which also increased the removal length of SWNTs. From SEM observations, SWNTs were categorized into two parts after the breakdown process; the SWNTs which disappeared (removed parts) and the SWNTs which still remained on the substrates (unremoved parts). Comparison of the heights of the removed parts in the white dashed box of Fig. 4(c) and the unremoved parts along the same SWNTs after breakdown in the molecular glass film indicated that the removed parts were thicker (on average, ca. 2.2 nm) than the unremoved parts (on average, ca. 0.7 nm). This implies that molecular glass around the m-SWNTs is locally involved in chemical reactions with SWNTs and consequently becomes insoluble in acetone. The heat of oxidation from the surrounding organic materials, in addition to that from the SWNT, could induce axially-spread oxidation of the SWNT itself. In contrast, the thickness of the parts where breakdown occurred in the PMMA film are smaller (on average, ca. 0.75 nm) than that of the unremoved parts (on average, ca. 1.5 nm) [Fig. 4(f)]. This confirmed the removal of SWNTs, although there was still undissolved soot from the SWNTs or PMMA. The oxidation of

PMMA could also induce long-length breakdown because the oxidation temperature of PMMA (ca. 304 °C) is lower than that of the SWNTs (500-700 °C[28]).

Another effect of the organic film is to prevent the SWNTs from rapid cooling after breakdown, because they are locally heated close to the SWNT temperatures by Joule heating of the SWNTs. This was supported by faster ramp-up voltage experiments in molecular glass films. When breakdown was performed with an increased ramp rate of drain voltage (ca. 4 V/s) so that the film did not become sufficiently hot, the removal length (100-300 nm) was almost the same as that for in-air breakdown (data not shown). The function of the organic materials as heat reservoirs is explained by their lower thermal diffusivity (for example, PMMA; ca. 1.1×10^{-7} m^2/s) than air (ca. 2.2×10^{-5} m^2/s) at room temperature.

Uniform power dissipation along the SWNTs is also important for their full-length removal. When the SWNTs assigned as semiconducting by RBM spectra were purposely broken with negative gate voltages and high drain voltages, the removal lengths tended to be smaller (<1.5 μm) than those of m-SWNTs (data not shown). Asymmetric power dissipation along an s-SWNT due to non-uniform electric field and charge density[29,30] was thus the probable cause of shorter-length SWNT removal. Kinks in the SWNTs that originated from growth or transfer processes also generated non-uniform temperatures[31] along the SWNT, and therefore resulted in partial breakdown (data not shown).

The maximum SWNT removal length and length consistency can be significantly improved by the appropriate selection of film materials in terms of their oxidation characteristics and thermal properties, or by reducing non-uniformity of power dissipation caused by kinks in the SWNTs. The amount of oxygen molecules that permeate through the organic films is also an important factor for oxidation reaction of the films and SWNTs; therefore, the selection of film material and thickness should be considered. Under optimized conditions, organic film-assisted breakdown can yield arrays of pure s-SWNTs with larger areas, where a great number of FETs with high on/off ratio can be fabricated by simply placing electrodes without further purification processes. Further multiple fabrication of FETs using the s-SWNT arrays purified by organic film-assisted electrical breakdown is currently underway. Device fabrication based on s-SWNT arrays would enable SWNT-based large-scale integrated circuits or other semiconducting devices to be obtained.

4 Conclusions

In summary, a new technique was developed for the selective removal of long lengths of m-SWNTs using electrical breakdown in two types of organic films. High removal selectivity was supported by the transfer characteristics of FETs and long-length removal of m-SWNTs in channel areas was confirmed by multiple analyses. A maximum removal length of 16.4 μm and spatial resolution of ca. 55 nm were attained, probably due to heat generation around the SWNTs by oxidation of the organic film and/or heat accumulation effect of the organic materials.

Acknowledgements

Part of this work was financially supported by Grants-in-Aid for Scientific Research (Nos. 22226006, 23760179, 25630063, 25107002) and the IRENA Project of JST-EC DG RTD, Strategic International Collaborative Research Program (SICORP). This work was partly conducted at the Center for Nano Lithography & Analysis, VLSI Design and Education Center (VDEC), and Laser Alliance, the University of Tokyo. K.O. was financially supported by the Iwadare Scholarship Foundation and Global Leader Program for Social Design and Management. T.I. was financially supported by a Japan Society for the Promotion of Science (JSPS) Fellowship (23-8717).

Notes and references

Department of Mechanical Engineering, The University of Tokyo, 7-3-1 Hongo, Bunkyo-ku, Tokyo 113-8656, Japan. E-mail: maruyama@photon.t.u-tokyo.ac.jp, chiashi@photon.t.u-tokyo.ac.jp; Fax: +81-3-5800-6983; Tel: +81-3-5841-6421

1 N. Patil, J. Deng, S. Mitra, and H. S. P. Wong, *IEEE Trans. Nanotechnol.*, 2009, **8**, 37–45.
2 M. M. Shulaker, G. Hills, N. Patil, H. Wei, H. Y. Chen, H. S. P. Wong, and S. Mitra, *Nature*, 2013, **501**, 526–530.
3 C. Kocabas, S. H. Hur, A. Gaur, M. A. Meitl, M. Shim, and J. A. Rogers, *Small*, 2005, **1**, 1110–1116.
4 H. Ago, K. Nakamura, K. Ikeda, N. Uehara, N. Ishigami, and M. Tsuji, *Chem. Phys. Lett.*, 2005, **408**, 433–438.
5 J. Li, K. Liu, S. Liang, W. Zhou, M. Pierce, F. Wang, L. Peng, and J. Liu, *ACS Nano*, 2014, **8**, 554–562.
6 S. W. Hong, T. Banks, and J. A. Rogers, *Adv. Mater.*, 2010, **22**, 1826–1830.
7 Y. Li, D. Mann, M. Rolandi, W. Kim, A. Ural, S. Hung, A. Javey, J. Cao, D. Wang, E. Yenilmez, Q. Wang, J. F. Gibbons, Y. Nishi, and H. Dai, *Nano Lett.*, 2004, **4**, 317–321.
8 G. Hong, B. Zhang, B. Peng, J. Zhang, W. M. Choi, J. Y. Choi, J. M. Kim, and Z. Liu, *J. Am. Chem. Soc.*, 2009, **131**, 14642–14643.
9 W. Zhou, S. Zhan, L. Ding, and J. Liu, *J. Am. Chem. Soc.*, 2012, **134**, 14019–14026.
10 X. Qin, F. Peng, F. Yang, X. He, H. Huang, D. Luo, J. Yang, S. Wang, H. Liu, L. Peng, and Y. Li, *Nano Lett.*, 2014, **14**, 512–517.
11 A. D. Franklin, *Nature*, 2013, **498**, 443–444.
12 M. S. Arnold, A. A Green, J. F. Hulvat, S. I. Stupp, and M. C. Hersam, *Nat. Nanotechnol.*, 2006, **1**, 60–65.
13 H. Liu, D. Nishide, T. Tanaka, and H. Kataura, *Nat. Commun.*, 2011, **2**, 309-316.
14 Q. Cao, S. Han, G. S. Tulevski, Y. Zhu, D. D. Lu, and W. Haensch, *Nat. Nanotechnol.*, 2013, **8**, 180–186.
15 M. Engel, J. P. Small, M. Steiner, M. Freitag, A. A. Green, M. C. Hersam, and P. Avouris, *ACS Nano*, 2008, **2**, 2445–2452.
16 B. K. Sarker, S. Shekhar, and S. I. Khondaker, *ACS Nano*, 2011, **5**, 6297–6305.
17 P. G. Collins, M. S. Arnold, and P. Avouris, *Science*, 2001, **292**, 706–709.

18 G. Zhang, P. Qi, X. Wang, Y. Lu, X. Li, R. Tu, S. Bangsaruntip, D. Mann, L. Zhang, and H. Dai, *Science*, 2006, **314**, 974–947.
19 G. Hong, M. Zhou, R. Zhang, S. Hou, W. Choi, Y. S. Woo, J. Y. Choi, Z. Liu, and J. Zhang, *Angew. Chem. Int. Ed.*, 2011, **50**, 6819–6823.
20 S. Li, C. Liu, P. X. Hou, D. M. Sun, and H. M. Cheng, *ACS Nano*, 2012, **6**, 9657–9661.
21 S. H. Jin, S. N. Dunham, J. Song, X. Xie, J. H. Kim, C. Lu, A. Islam, F. Du, J. Kim, J. Felts, Y. Li, F. Xiong, M. A. Wahab, M. Menon, E. Cho, K. L. Grosse, D. J. Lee, H. U. Chung, E. Pop, M. A. Alam, W. P. King, Y. Huang, and J. A. Rogers, *Nat. Nanotechnol.*, 2013, **8**, 347–355.
22 S. Maruyama, R. Kojima, Y. Miyauchi, S. Chiashi, and M. Kohno, *Chem. Phys. Lett.*, 2002, **360**, 229-234.
23 S. Chiashi, H. Okabe, T. Inoue, J. Shiomi, T. Sato, S. Kono, M. Terasawa, and S. Maruyama, *J. Phys. Chem. C*, 2012, **116**, 6805–6808.
24 T. Inoue, D. Hasegawa, S. Badar, S. Aikawa, S. Chiashi, and S. Maruyama, *J. Phys. Chem. C*, 2013, **117**, 11804–11810.
25 L. Jiao, B. Fan, X. Xian, Z. Wu, J. Zhang, and Z. Liu, *J. Am. Chem. Soc.*, 2008, **130**, 12612–12613.
26 P. T. Araujo, S. K. Doorn, S. Kilina, S. Tretiak, E. Einarsson, S. Maruyama, H. Chacham, M. A. Pimenta, and A. Jorio, *Phys. Rev. Lett.*, 2007, **98**, 067401-067404.
27 R. Y. Zhang, Y. Wei, L. A. Nagahara, I. Amlani, and R. K. Tsui, *Nanotechnology*, 2006, **17**, 272–276.
28 Y. Murakami, Y. Miyauchi, S. Chiashi, and S. Maruyama, *Chem. Phys. Lett.*, 2003, **374**, 53–58.
29 A. Liao, R. Alizadegan, Z. Y. Ong, S. Dutta, F. Xiong, K. J. Hsia, and E. Pop, *Phys. Rev. B*, 2010, **82**, 205406-205409.
30 C. L. Tsai, A. Liao, E. Pop, and M. Shim, *Appl. Phys. Lett.*, 2011, **99**, 053120-3.
31 X. Xie, K. L. Grosse, J. Song, C. Lu, S. Dunham, F. Du, A. E. Islam, Y. Li, Y. Zhang, E. Pop, Y. Huang, W. P. King, and J. A. Rogers, *ACS Nano*, 2012, **6**, 10267–10275.